Original Articles

Acupuncture and Herbal Medicine

Ginseng and Rhubarb combination ameliorates ferroptosis in persistent inflammation, immunosuppression, and catabolism syndrome *via* the CaMKII/HO-1 signaling pathway

Yiming Wei[1,2,3], Xiaomeng Guo[1,3,4], Yahui Hu[1,3], Yake Li[1,3], Tengfei Chen[1], Chang Liu[5], Lixuan Zhang[6], Qing Ye[7], Qingquan Liu[1,3,4,*], Xiaolong Xu[1,3,4,*]

[1]Beijing Hospital of Traditional Chinese Medicine, Capital Medical University, Beijing, China; [2]Xiamen Traditional Chinese Medicine Hospital, Xiamen, China; [3]Beijing Institute of Chinese Medicine, Beijing, China; [4]Beijing Key Laboratory of Innovative Research on Removing Stasis and Detoxification Theory in Infectious Diseases, Beijing, China; [5]Center for Health Policy and Technology Evaluation, Peking University Health Science Center, Beijing, China; [6]Beijing University of Chinese Medicine Third Affiliated Hospital, Beijing, China; [7]Beijing Changping District Hospital of Integrated Traditional Chinese and Western Medicine, Beijing, China

Abstract

Objective: This study aimed to investigate the therapeutic effects and underlying mechanisms of the Ginseng and Rhubarb combination (GRC) on sepsis-induced persistent inflammation, immunosuppression, and catabolism syndrome (PICS).

Methods: The mouse model of sepsis-induced PICS was established using cecal ligation and puncture (CLP). Mice were randomly assigned to five groups: sham, model, model + GRC, model + GRC + oleic acid (OA), and model + GRC + celastrol (CELA). GRC was administered by oral gavage once daily for 7 days, whereas the agonists were injected intraperitoneally for 3 days. Additionally, KN-93 (a calcium/calmodulin-dependent protein kinase II [CaMKII] inhibitor; 5 mg/kg) was used to verify the inhibitory regulation of CaMKII signaling. Seventy-two hours after surgery, serum and tissue samples were collected to evaluate the therapeutic effects of GRC. Outcome measures included survival, body weight, splenic immune cell distribution, histopathology, inflammatory cytokine levels, and ferroptosis-related indicators. Targeted metabolomics and data-independent acquisition (DIA)–based proteomics were performed to identify differential molecules and pathways associated with GRC treatment.

Results: Compared to the model group, GRC markedly improved the survival rate and mitigated body weight loss in septic PICS mice. GRC reduced splenic neutrophil and macrophage infiltration and increased the proportions of $CD4^+$ and $CD8^+$ T cells. Histopathological examination revealed attenuation of organ damage. Levels of inflammatory cytokines (interleukin [IL]-6, tumor necrosis factor-alpha (TNF-α), IL-4, IL-13) were significantly decreased, and metabolic disturbances were ameliorated. Biochemical assays showed that GRC reduced Fe^{2+} and malondialdehyde (MDA) levels while increasing glutathione peroxidase (GSH-PX) and GPX4, indicating inhibition of ferroptosis. Western blot (WB) analysis demonstrated that GRC downregulated the CaMKII/heme oxygenase-1 (HO-1) pathway, and this regulatory effect was reversed by CaMKII and HO-1 agonists. Multi-omics analysis further revealed that GRC modulated metabolic and proteomic networks associated with immune regulation and ferroptosis, confirming that its therapeutic benefits were mediated through suppression of the CaMKII/HO-1/GPX4 axis.

Conclusions: GRC exhibited significant anti-inflammatory, immunomodulatory, and organ-protective effects in the murine model of sepsis-induced PICS. These benefits were mediated through the suppression of ferroptosis *via* modulation of the CaMKII/HO-1 pathway, providing a novel experimental foundation and a potential therapeutic strategy for managing sepsis-associated PICS.

Keywords: Ferroptosis, Ginseng, PICS, Rhubarb, Sepsis, CaMKII/HO-1/GPX4 axis

Graphical Abstract: https://links.lww.com/AHM/A206

Introduction

Sepsis, a life-threatening organ failure caused by a dysfunctional response to infection, is a major threat to global health. Approximately 48.9 million cases and 11 million sepsis-related deaths were recorded worldwide in 2017, accounting for 19.7% of global deaths[1]. The incidence of sepsis in the intensive care unit (ICU) in China was 20.6 per 100 ICU admissions, with a 90-day

Yiming Wei and Xiaomeng Guo are contributed equally to this work.

**Corresponding author. Xiaolong Xu, E-mail: xiaolong_xu3013@126.com; Qingquan Liu, E-mail: liuqingquan_2003@126.com.*

How to cite this article: *Wei YM, Guo XM, Hu YH, Li YK, Chen TF, Liu C, Zhang LX, Ye Q, Liu QQ, Xu XL. Ginseng and Rhubarb combination ameliorates ferroptosis in persistent inflammatory immunosuppressed catabolic syndrome via the CaMKII/HO-1 signaling pathway. Acupunct Herb Med 2026;6(2):205–219. doi: 10.1097/HM9.0000000000000183*

Received 20 June 2025 / Accepted 23 January 2026

Copyright © 2026 Tianjin University of Traditional Chinese Medicine. This is an open-access article distributed under the terms of the Creative Commons Attribution-Non Commercial-No Derivatives License 4.0 (CCBY-NC-ND), where it is permissible to download and share the work provided it is properly cited. The work cannot be changed in any way or used commercially without permission from the journal.

HM9_V6N2.indb 205 25-Jun-26 00:44:57

mortality rate of 35.5%[2]. The mortality rate associated with sepsis is closely related to factors such as advanced age, low body weight, inflammation, and immunosuppression[2]. The high mortality rate is further linked to persistent inflammation, immune dysfunction, and metabolic disturbances, highlighting the urgent need for effective therapeutic strategies.

Exploration of the pathophysiological characteristics of sepsis has garnered considerable research interest. Progressing from systemic inflammatory response syndrome (SIRS) to compensatory anti-inflammatory response syndrome (CARS) and further evolving into mixed anti-inflammatory response syndrome (MARS), researchers have incrementally deepened their understanding. Previous studies have highlighted the concurrent presence of hyperinflammation and immunosuppression throughout the course of sepsis[3–6]. Distinguishing between these states proves challenging, with no clear transition from the pro-inflammatory to the anti-inflammatory stage[7–8]. Based on the "SIRS-CARS-MARS" model, scholars have proposed the concept of persistent inflammatory immunosuppressed catabolic syndrome (PICS), which is characterized by persistent hyperinflammation and immunosuppression and leads to high decomposition of fat and protein, resulting in complications such as organ failure and nosocomial infection. Currently, PICS is the latest and most comprehensive pathological summary of late-stage sepsis leading to progressive organ dysfunction and poor late outcomes; therefore, caution should be exercised[9]. Despite studies on the pathology and biomarkers of PICS, research into its treatment remains in its nascent stage[10].

Recent studies have identified ferroptosis, an iron-dependent form of regulated cell death driven by lipid peroxidation, as a key mechanism underlying organ failure in sepsis[11–13]. Ferroptosis contributes to immune dysregulation, oxidative stress, and metabolic imbalance[14], which closely mirror the pathological features of PICS. In particular, the aberrant activation of the calcium/calmodulin-dependent protein kinase II (CaMKII) and heme oxygenase-1 (HO-1) signaling pathways has been implicated in ferroptosis-mediated tissue injury[5]. However, the role of ferroptosis and its regulatory signaling in PICS remains largely unexplored, warranting further mechanistic investigation.

Presently, there is a lack of specific drugs for PICS, so treatment generally involves a combination strategy. This currently focuses on addressing the primary disease, modulating inflammation, and providing immunotherapy and nutritional support[15]. Traditional Chinese medicine (TCM) has emerged as a pivotal approach in critical illness treatment and has received increased attention for its significant contributions during the COVID-19 pandemic[16]. Notably, GRC, composed of *Panax ginseng* C. A. Mey and *Rheum palmatum* L. [Supplementary Table S1, https://links.lww.com/AHM/A207], holds prominence in clinical applications. Both ginseng and rhubarb have shown protective effects in alleviating organ dysfunction, controlling inflammatory storms, boosting immune function, and regulating gut microbiota and metabolic imbalance, thereby improving the prognosis of sepsis[3–6]. This study employed GRC rather than single herb administration, which better aligns with clinical practice and provides a valuable reference for clinical treatment. Building on this, further animal experiments combined with multi-omics analysis were conducted to elucidate the underlying mechanisms and validate the findings. Ultimately, GRC may represent a potential therapeutic candidate for sepsis-induced PICS.

Materials and methods

Drugs and reagents

Ginseng and Rhubarb combination (GRC) was prepared in the form of formula granules provided by Beijing Chunfeng Traditional Chinese Medicine Co., Ltd. (Beijing, China). Oleic acid (OA, HY-N1446), Celastrol (CELA, IC0220), and KN-93 (HY-15465) were obtained from MedChemExpress (Monmouth Junction, NJ, USA). Corn oil (IC9000), dimethyl sulfoxide (DMSO, D8371), and the ferrous ion content assay kit (BC5415) were purchased from Beijing Solarbio Science & Technology Co., Ltd. (Beijing, China). Radioimmunoprecipitation assay (RIPA) lysis buffer (C1053+), protease inhibitor cocktail (P1266), phosphatase inhibitor cocktail (P1260), and protein-loading buffer (P1043) were obtained from Applygen Technologies Inc. (Beijing, China). The bicinchoninic acid (BCA) protein assay kit (23227) and Th1/Th2 cytokine 11-plex assay kit (EPX110-20820-901) were purchased from Thermo Fisher Scientific (Waltham, MA, USA). Rabbit monoclonal antibodies (mAb) against GPX4 (A11243), CaMKII (A0198), and HO-1 (A19062) were purchased from ABclonal Technology Co., Ltd. (Wuhan, China). Antibodies against interleukin-10 (IL-10, GB11108), GAPDH (GB15004), and β-actin (GB15003) were obtained from Servicebio Technology Co., Ltd. (Wuhan, China). Goat anti-rabbit IgG (H + L) HRP conjugate (S0101) and enhanced chemiluminescence (ECL) hypersensitive luminescent solution (E1060) were purchased from LabLead Biotechnology Co., Ltd. (Beijing, China). Rabbit monoclonal antibodies against IL-6 (ab290735), tumor necrosis factor-alpha (TNF-α, ab183218), and transforming growth factor-β (TGF-β, ab215715) were purchased from Abcam plc (Cambridge, UK). Rapid blocking buffer for western blotting (P0252) and Mouse IL-6 (PI326), Mouse TNF-α (PT512), Mouse IL-4 (PI612), and Mouse IL-13 (PI539) enzyme-linked immunosorbent assay (ELISA) kits were purchased from Beyotime Biotechnology Co., Ltd. (Shanghai, China). Anti-mouse CD45, CD3e, CD4, CD8a, anti-human/mouse CD11b, and anti-mouse F4/80 antibodies were obtained from Cytek Biosciences Inc. (Fremont, CA, USA). The stripping buffer (01427) was purchased from CWBIO Biotechnology Co., Ltd. (Jiangsu, China). The malondialdehyde (MDA) detection kit (A003-1-1) and glutathione peroxidase (GSH-PX assay kit; A005-1-1) were obtained from Nanjing Jiancheng Bioengineering Institute (Nanjing, China).

Animal experiments

Specific pathogen-free male C57BL/6J mice (6 weeks old, 20–23 g body weight) were purchased from Beijing Huafukang Biotechnology Co., Ltd (SCXK [Beijing] 2024-0003) and raised by the Beijing Institute of

HM9_V6N2.indb 206 25-Jun-26 00:44:57

Traditional Chinese Medicine (Beijing, China) under standard conditions for pure line animals. Experiments were conducted after 1 week of adaptive feeding. All experiments involving mice were performed in accordance with the ethical guidelines approved by the Animal Ethics Society of Beijing Hospital of Traditional Chinese Medicine Affiliated to Capital Medical University (BJTCM-M-2024-02-10).

The mice were randomly divided into sham and model groups. Mice were anesthetized with 1% sodium pentobarbital. Cecal ligation and puncture (CLP) was performed to establish a sepsis-induced PICS model. After anesthetizing the mice, their abdominal area was disinfected with alcohol swabs. A midline incision was made just below the xiphoid process, cutting through both the skin and abdominal wall. The abdominal cavity was opened, and the cecum was located and carefully extracted. In the sham group, the cecum was returned to the abdominal cavity, and the incision was sutured without further manipulation. For the CLP procedure, the base of the cecum was ligated, and the upper part of the cecum was punctured using a 20-gauge (20G) needle. After squeezing out the feces, the cecum was returned to the abdominal cavity. The incision was then closed layer by layer, and fluid resuscitation was performed by subcutaneously injecting 2 mL of physiological saline into the nape of the mouse. Sham mice underwent only laparotomy to locate the cecum and did not undergo cecal ligation or puncture. Model success was verified by weight loss, increased mortality, and immunologic/metabolic abnormalities at 72 hours post-surgery.

Based on the daily GRC dose used in patients, the converted daily GRC dose for mice was calculated to be 20.475 g/kg. Four dosage gradients were established (3 times, 1 time, 1/3 times, and 1/9 times this amount) for drug screening, and the dosage providing the highest survival rate 7 days after CLP was selected. The daily gavage volume for the mice was 0.5 mL, and the granules were dissolved in pure water to a concentration of 0.81 g/mL. Mice were administered GRC (20.475 g/kg) by oral gavage once daily for 7 days after CLP. Sham mice received equivalent volumes of normal saline. Mouse survival and body weight were recorded daily after CLP. To obtain medicated serum, mice received GRC by oral gavage for 7 days without CLP surgery, and serum was collected 30 or 60 min after gavage on the seventh day.

For the CaMKII/HO-1 verification test, mice were randomly divided into the following groups: sham, model, model + GRC, model + GRC + OA, and model + GRC + CELA. Mice were intraperitoneally injected with 0.1 mL OA (5 μM) and 0.1 mL CELA (1 mg/kg) separately, 7 days before establishing the PICS model.

To further validate the involvement of CaMKII signaling in GRC-mediated protection, we performed an additional intervention using the CaMKII inhibitor KN-93. Mice were randomly assigned to six groups: control, sham, model, model + GRC, model + KN-93, and model + GRC + KN-93. KN-93 was administered intraperitoneally at 5 mg/kg once daily for two consecutive days, beginning 24 hours before CLP. After the interventions, the mice were euthanized, and tissues were collected.

Metabolomics

Mice serum was analyzed using targeted metabolomics. Targeted metabolomics was performed using ultra-performance liquid chromatography (UPLC) (ExionLCTM AD; SCIEX, Shanghai, China) coupled with tandem mass spectrometry (MS/MS) (Applied Biosystems 6500 QTRAP; SCIEX) to detect metabolites[17]. The software Analyst 1.6.3 was used to process the mass spectrum data. Metabolites were quantified by multiple reaction monitoring (MRM) on a triple quadrupole mass spectrometer[18]. Metabolomics HM400 (a high-throughput targeted metabolome) was performed using LC-MS QTRAP 6500+ (SCIEX) and high-performance liquid chromatography-tandem mass spectrometry (LC-MS/MS)[19]. Data analysis methods included partial least squares-discriminant analysis (PLS-DA)[20] and orthogonal partial least squares-discriminant analysis (OPLS-DA)[21]. The OPLS-DA function from the MetaboAnalyst package in R was used for analysis.

Network pharmacology

The metabolites identified through metabolomic analysis of the medicated serum were considered active constituents of the GRC-treated serum. The potential targets of these components were retrieved from the TCMSP and DrugBank databases. Gene identifiers were converted using the UniProtKB database. Sepsis-related disease targets were collected from the GeneCards and OMIM databases, retaining only those with scores above the median. Core targets were identified as the intersection of drug- and sepsis-related targets. These intersecting targets were submitted to the STRING platform to construct a protein–protein interaction (PPI) network. Key PPI targets were identified using MCODE in Cytoscape (version 3.9.1). Gene Ontology (GO) and Kyoto Encyclopedia of Genes and Genomes (KEGG) pathway enrichment analyses were performed using the Metascape database.

DIA proteomics

Mouse serum samples were subjected to proteomic analysis using a label-free quantitative proteomics approach. Mass spectrometry data were acquired in Orbitrap Fusion Lumos (Thermo Fisher Scientific, San Francisco, CA, USA). Following DIA data deconvolution, peptide and protein identification and quantification were performed. The ion peak areas extracted from the experimental spectra were processed using the MSstats package for error correction and normalization. Differential protein expression was assessed based on predefined comparison groups using a linear mixed-effects model, followed by functional analysis of the identified proteins.

Joint analysis of metabolomics and proteomics

The relative abundances of metabolites and proteins were used to calculate correlation coefficients after data

HM9_V6N2.indb 207 25-Jun-26 00:44:57

normalization. Univariate correlations were assessed using Spearman's rank correlation analysis implemented in the corr. Test R package. For unsupervised modeling, principal component analysis (PCA) was performed separately and jointly on the proteomic and metabolomic datasets. Canonical correlation analysis (CCA) was conducted using the Metware platform to evaluate global-level associations between differential metabolites and proteins. Biological functional associations were investigated using KEGG pathway enrichment analysis of differentially expressed proteins and metabolites.

Hematoxylin–eosin staining

Mouse tissues (lung, heart, liver, spleen, and kidney) were fixed in 4% paraformaldehyde for more than 24 hours. The tissues were dehydrated, embedded in paraffin, sectioned at a thickness of 3 μm using a rotary microtome, and stained with hematoxylin and eosin (H&E).

Flow cytometry

Single-cell suspensions were prepared from murine spleens and counted using an automated cell counter. The cell aliquots were then distributed into centrifuge tubes. Specific antibody panels were used to identify distinct immune cell populations. $CD4^+$ T cells were labeled with CD45, CD3, and CD4 antibodies; $CD8^+$ T cells with CD45, CD3, and CD8 antibodies; and macrophages with CD45, CD11b, and F4/80 antibodies. Following a 15-min incubation with the corresponding antibody cocktails at 4 °C, cells were washed with phosphate-buffered saline (PBS) and analyzed using a BD Biosciences flow cytometer, with subsequent data processing performed using FlowJo software (version: 10.8.1, Aurora; Cytek® Biosciences, Fremont, CA, USA).

Enzyme-linked immunosorbent assay

Serum samples were collected from all groups of mice, and the concentrations of pro-inflammatory cytokines (IL-6, TNF-α) and anti-inflammatory cytokines (IL-4, IL-13) were quantitatively determined using ELISA kits according to the manufacturer's protocols.

Multifactor microarray

Cytokines in mouse serum, including IL-12, IL-13, IL-1β, IL-2, IL-4, IL-5, IL-6, TNF-α, and IL-18, were detected using Luminex 200, MAGPIX and FlexMAP3D systems. Final concentrations were calculated by interpolation using a five-parameter logistic model.

Western blot

Mouse lung tissues were treated with RIPA lysis buffer, protease inhibitor, and phosphatase inhibitor, and left to stand for 30 min after shaking. The supernatant was collected after centrifugation at 4°C and 12,000 rpm for 10 min. Proteins were separated using 10% or 12% sodium dodecyl sulfate-polyacrylamide gel electrophoresis (SDS-PAGE) and transferred to a polyvinylidene fluoride (PVDF) membrane. The membrane was blocked with the rapid blocking buffer for 30 min and incubated with primary antibodies (GPX4, CaMKII, and HO-1) on a shaker at 4°C for 12 to 18 hours. After washing with Tris-buffered saline, the membrane was incubated with secondary antibody at room temperature for 45 min. After cleaning, the ECL hypersensitive luminescent solution was used for imaging. Stripping buffer was applied to remove antibodies, and the reference antibody was re-incubated.

Biochemical detection

Mouse lung tissue was homogenized with physiological saline and steel beads and centrifuged at 3,000 rpm for 10 min. The supernatant was used to prepare a 10% tissue homogenate. For MDA detection, the samples were mixed with the working solution and incubated in a 95°C water bath for 40 min. After cooling, the mixture was centrifuged at 10,000 g for 10 min, and the absorbance at 532 nm was measured to determine MDA content. For the GSH-PX assay, the samples were incubated with GSH reagent at 37°C in a water bath. After incubation, the mixture was centrifuged at 4,000 rpm for 10 min, and the absorbance at 421 nm was measured to calculate enzyme activity. For Fe^{2+} concentration determination, the samples were mixed with the reagent, centrifuged at 12,000 rpm for 10 min, and the absorbance was measured at 593 nm.

Statistical analysis

Statistical analyses were performed using GraphPad Prism software (version 9.0.0; San Diego, CA, USA). Data normality was assessed using the Shapiro-Wilk test. For normally distributed data, comparisons between two groups were analyzed using a two-tailed Student's *t* test, while comparisons among three or more groups were performed using one-way analysis of variance (ANOVA) followed by Tukey's *post hoc* test. Nonparametric tests were applied for non-normally distributed data: the Mann-Whitney *U* test for two-group comparisons and the Kruskal-Wallis test with Dunn's *post hoc* analysis for three or more groups. For multiple measurements from the same mouse, two-way repeated-measures ANOVA with a single pooled variance was used, applying Tukey's correction for pairwise comparisons within groups. Statistical significance was set at $P \leq 0.05$ (two-tailed test).

Results

The construction of the animal model of sepsis-induced PICS was confirmed through persistent inflammation, immunosuppression, and metabolic dysregulation

In model mice, the mortality rate increased significantly within 48 hours after CLP surgery. The total number of deaths gradually decreased within 72 hours, and no additional deaths occurred after the fourth day of the pathophysiological state post-CLP surgery. Compared with the sham group, the survival rate of mice in the model group decreased significantly ($P = 0.001$; Figure 1A). The body weight of mice in the model group declined persistently during the first 4 days post-CLP, followed by a gradual upward trend (Figure 1B). Inflammation

HM9_V6N2.indb 208 25-Jun-26 00:44:57

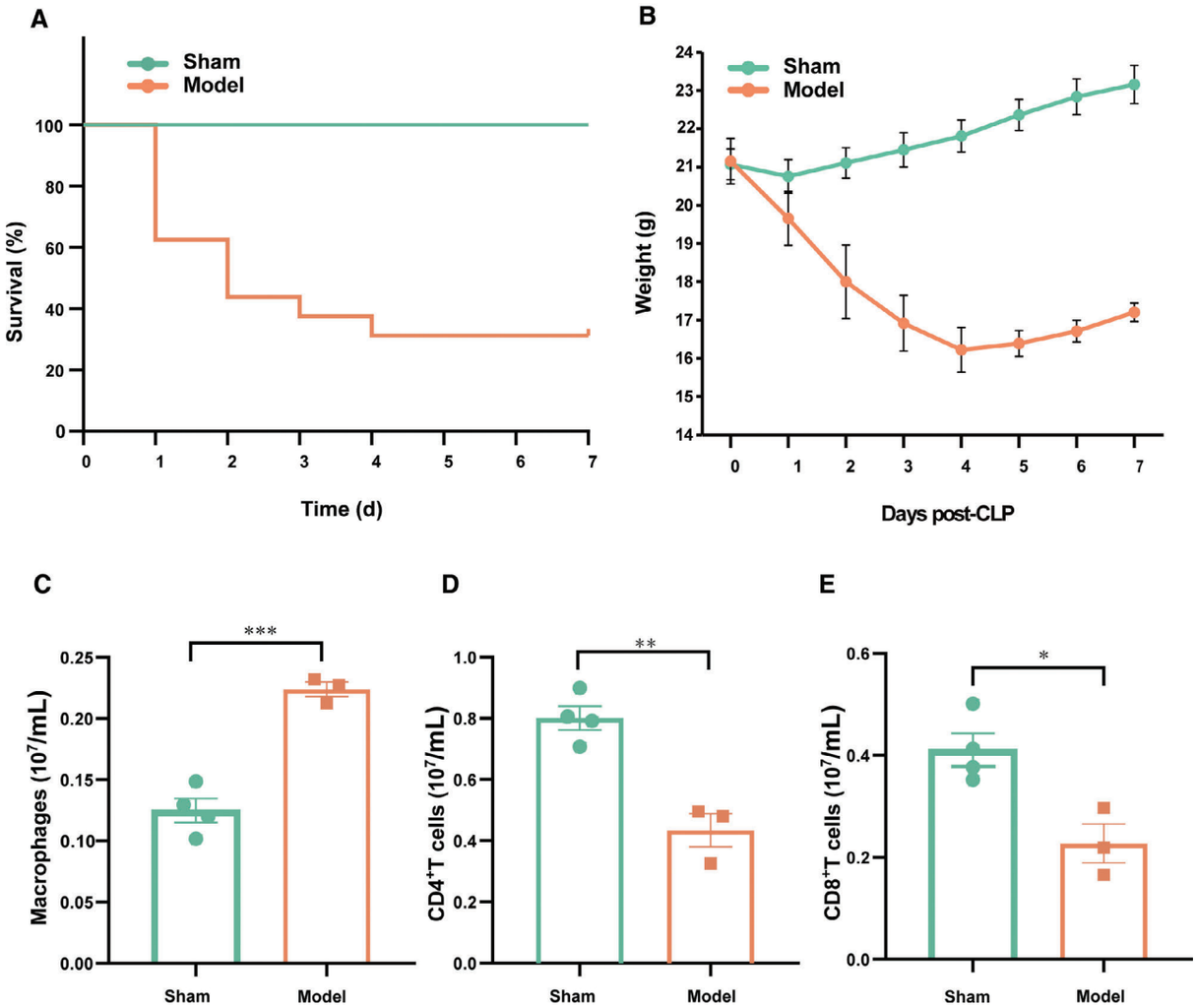


Figure 1. CLP-induced mice exhibited persistent inflammation, immunosuppression, and metabolic dysregulation characteristic of PICS. (A) Kaplan-Meier survival curves over a 7-day period in the sham and model groups. (B) Body weight changes throughout the 7-day experimental period. (C–E) Quantification of splenic macrophages (C), $CD4^+$ T cells (D), and $CD8^+$ T cells (E). *$P < 0.05$, **$P < 0.01$, ***$P < 0.001$. CLP: Cecal ligation and puncture; PICS: Persistent inflammatory immunosuppressed catabolic syndrome.

was evident from an increased number of splenic macrophages in the model group ($P = 0.001$; Figure 1C). Immunosuppression was indicated by a reduced number of $CD4^+$ and $CD8^+$ T cells in the spleens of the model group ($P < 0.05$; Figure 1D, E). The 7-day mortality analysis revealed that most deaths occurred before the fourth or fifth day, with no additional deaths, suggesting that the third day marked the late stages of sepsis. Moreover, the downward trend in body weight was observed at 72 hours, indicating a state of metabolic imbalance. An excessive population of macrophages reflected heightened inflammation, whereas a diminished number of T cells indicated immunosuppression. These findings confirmed that the model met the criteria for persistent inflammation, immunosuppression, and metabolic derangement in a sepsis-related PICS model[22].

GRC exerts therapeutic effects in PICS mice by correcting inflammation and alleviating pathological organ damage

After the 7-day survival monitoring period, GRC-treated mice exhibited significantly increased survival rates ($P < 0.0001$; Figure 2A). GRC-treated mice showed a significant increase in body weight compared to PICS mice, with weight gradually increasing after 72 hours ($P < 0.001$; Figure 2B). Regarding inflammation and immune response, the spleens of GRC-treated mice contained a reduced population of macrophages compared to those of PICS-treated mice (Figure 2C). Conversely, GRC-treated mice exhibited higher counts of $CD4^+$ and $CD8^+$ T cells than PICS-treated counterparts (Figure 2D, E). Serum analysis revealed elevated levels of pro-inflammatory cytokines, including IL-6 and TNF-α (Figure 2F, G), as well as increased anti-inflammatory cytokines such as IL-4 and IL-13 in PICS mice (Figure 2H, I). Intriguingly, GRC treatment led to a decrease in both pro-inflammatory and anti-inflammatory cytokines. Similar trends were observed in liver cytokines, where pro-inflammatory cytokines IL-6 and TNF-α, along with anti-inflammatory cytokines IL-10 and TGF-β, surged in PICS mice but significantly decreased with GRC treatment (Figure 2O–S). The cytokine response in the PICS serum exhibited a less pronounced shift than the alterations observed in the PICS liver. H&E

HM9_V6N2.indb 209 25-Jun-26 00:44:58

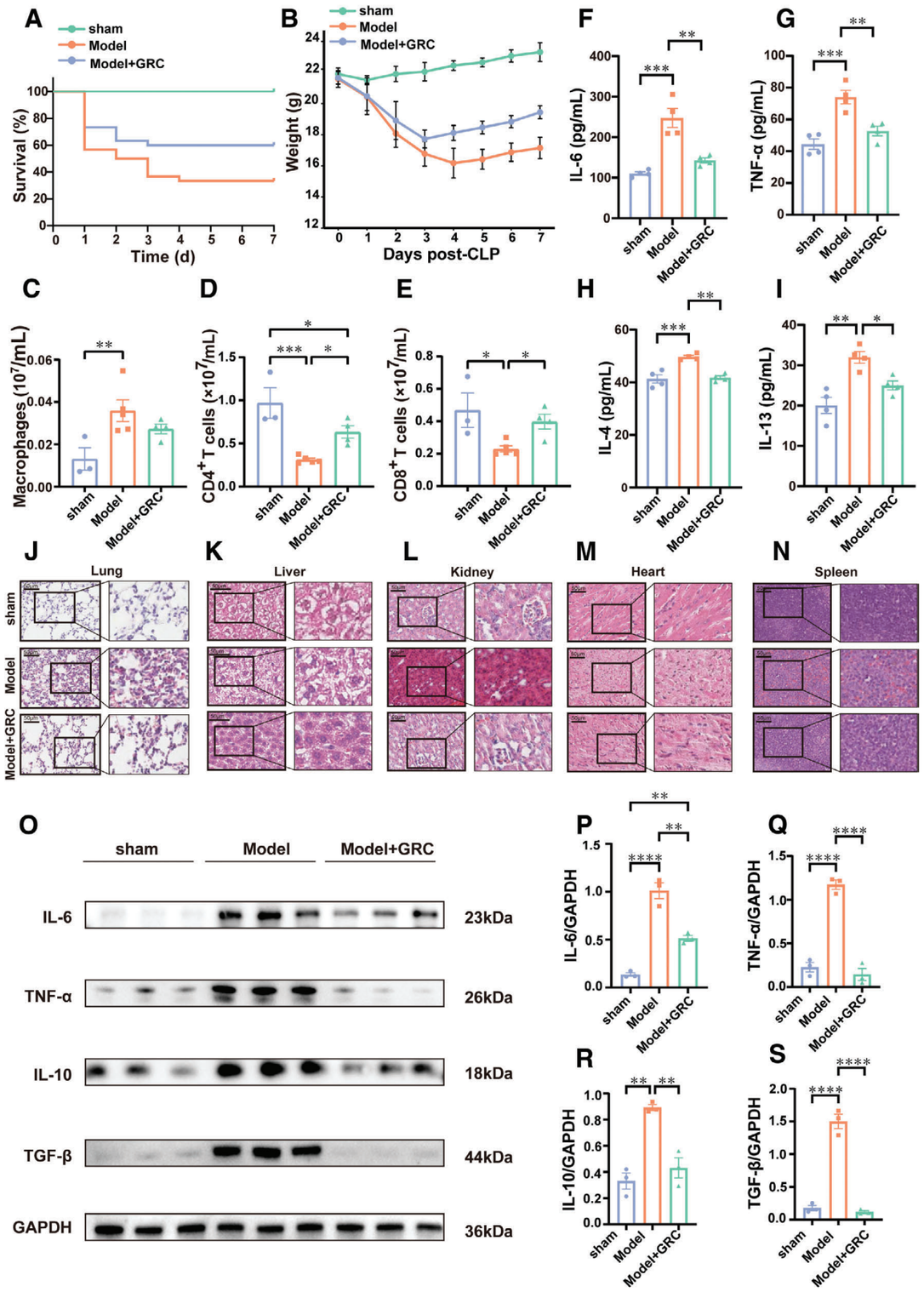


Figure 2. GRC improved the survival rate of PICS mice, corrected inflammation, and alleviated pathological organ damage. (A) Kaplan-Meier survival curves over 7 days. (B) Body weight changes throughout the 7-day experimental period. (C–E) Quantification of splenic macrophages (C), $CD4^+$ T cells (D), and $CD8^+$ T cells (E). (F–I) Serum levels of IL-6 (F), TNF-α (G), IL-4 (H), and IL-13 (I). (J–N) Representative histopathological images of the lung (J), liver (K), kidney (L), heart (M), and spleen (N). (O–S) Hepatic levels of IL-6 (O), TNF-α (P), IL-10 (Q), and TGF-β (S). $^*P < 0.05$, $^{**}P < 0.01$, $^{***}P < 0.001$, $^{****}P < 0.0001$. GRC: Ginseng and Rhubarb Combination; IL: Interleukin; PICS: Persistent inflammatory immunosuppressed catabolic syndrome; TGF-β: Transforming growth factor-β; TNF-α: Tumor necrosis factor-alpha.

staining revealed a compromised lung structure in PICS mice, characterized by a thickened alveolar septum and pronounced inflammatory cell infiltration. GRC-treated mice displayed restoration of lung architecture, mitigation of alveolar septal thickening, and reduction of inflammatory cell infiltration. Additionally, PICS mice

HM9_V6N2.indb 210 25-Jun-26 00:44:59

exhibited severe cardiomyocyte proliferation, which was alleviated by GRC treatment. Kidney tissues from PICS mice displayed impaired glomeruli and congestion; however, GRC treatment facilitated glomerular structure restoration and reduced congestion. Disruption of liver cell structure and pale spleen staining were evident in PICS mice but were ameliorated by GRC treatment (Figure 2J–N).

Integrated analysis of UPLC-MS/MS–based medicated serum components and network pharmacology reveals potential targets and pathways of GRC against sepsis

A comprehensive metabolomic analysis using UPLC-MS/MS identified 879 metabolites, including 13 class I metabolites (Figure 3A). These metabolites showed significant intergroup variations and formed five distinct clusters (Figure 3G). The separation trend among the groups was further confirmed using OPLS-DA score plots (Figure 3C, D), with model quality assessment indicating no risk of overfitting (Figure 3E, F). Differential metabolites were screened using criteria of variable importance in projection (VIP) ≥ 1 and fold change (FC) ≥2 or ≤0.5. By comparing blank serum with serum samples collected 30 and 60 min after GRC administration, 192 components were identified as medicated serum constituents, including key compounds such as ginsenoside Rs3, rheic acid, and chrysophanol (Figure 3J and Supplementary Table S2, https://links.lww.com/AHM/A208).

Through retrieval from the TCMSP and DrugBank databases, 255 target genes associated with the medicated components were predicted. In addition, 2,149 sepsis-related targets were obtained from the GeneCards and OMIM databases. The intersection of these datasets yielded 105 core targets (Figure 3B). The PPI network analysis of these core targets revealed that genes including *CCL2, IL-10, IL-6, PTGS2, IL-1β, TNF, IFNG, TP53, ICAM-1, CASP3, VEGF-A, IL-4, TGFB1, and HMOX1* played important roles in GRC intervention against sepsis (Figure 3H). Functional annotation indicated that these core targets were primarily involved in biological processes such as inflammatory response, hypoxia response, bacterial infection, and cytokine activity (Figure 3K). Furthermore, KEGG pathway analysis showed significant enrichment in the IL-17, TNF, Toll-like receptor, and hypoxia-inducible factor-1 (HIF-1) signaling pathways, suggesting that these pathways are central to the molecular mechanisms of GRC against sepsis (Figure 3I).

UPLC-MS/MS–based metabolomics analysis reveals the mechanism of GRC in regulating key metabolic pathways in PICS mice

Using the HM400 metabolomics platform, 418 serum metabolites were identified and quantitatively analyzed [Supplementary Figure S2, https://links.lww.com/AHM/A209]. PLS-DA revealed a clear separation in the metabolic profiles among the three groups (Figure 4A, B), indicating significant differences in metabolic states under different treatment conditions. Permutation test validation further confirmed the robustness of the PLS-DA model, showing no risk of overfitting (Figure 4C, D). Based on predefined criteria (FC ≥1.2 or ≤0.83, and $P < 0.05$), differential metabolites between groups were screened using univariate statistical analysis (Figure 4E and Supplementary Figure S3, https://links.lww.com/AHM/A209). Specifically, compared to the sham group, the PICS model group exhibited 39 significantly upregulated and 51 significantly downregulated metabolites, suggesting substantial metabolic dysregulation in the PICS state. After GRC intervention, nine metabolites were upregulated, and 14 were downregulated compared to the PICS model group (Figure 4F), indicating that GRC partially reverses PICS-induced metabolic abnormalities.

To further investigate the metabolic mechanism underlying the efficacy of GRC therapy, we focused on metabolites showing reversed trends in the comparisons between the model and sham groups and between the GRC-treated and model groups. Metabolites that normalized following GRC intervention after being dysregulated in PICS were potential mediators of its therapeutic effect. Detailed analysis showed that 2-deoxyglucose, 5-aminopentanoic acid, carnitine, and L-proline were significantly elevated in PICS mice but markedly reduced after GRC treatment, suggesting that GRC may alleviate metabolic stress and energy imbalance by regulating these metabolites. Conversely, 4-hydroxyphenylpyruvic acid, oxoadipic acid, and sebacic acid, which were suppressed in the PICS state, were significantly increased after GRC intervention, indicating that GRC also promoted the recovery of amino acid and fatty acid metabolism pathways. In summary, these findings demonstrated that GRC significantly modulates metabolic remodeling in PICS mice, which may represent an important mechanism for alleviating sepsis-associated metabolic disorders.

DIA-based proteomics reveals reversal of aberrant key protein expression by GRC in PICS mice

Using DIA-based proteomics, we identified 12,957 peptides and 1,457 proteins. Protein molecular weights were primarily concentrated in the 10 to 50 kDa range, with coverage rates generally below 80% [Supplementary Figure S4, https://links.lww.com/AHM/A209]. PCA showed a clear separation between the protein expression profiles of the PICS model and sham groups, and a distinct separation trend was also observed between the GRC-treated and model groups (Figure 5B). Using thresholds of FC ≥2 or ≤0.05 and $P < 0.05$, significantly differentially expressed proteins were screened (Figure 5C–E). Compared with the sham group, the PICS model group exhibited 63 upregulated and 25 downregulated proteins, whereas the GRC-treated group showed 16 upregulated and 59 downregulated proteins relative to the model group (Figure 5A).

Key proteins displayed reversed expression trends between the groups: FABP4, SNRPG, sorbitol dehydrogenase, AKR1D1, and PAI1, which were upregulated in the PICS model, were downregulated after GRC intervention. In contrast, IGLC3 and Ig γ-3 κ chain, which were downregulated in the model group, were significantly restored after treatment, demonstrating the reversal effect of GRC on aberrant protein expression in PICS.

HM9_V6N2.indb 211 25-Jun-26 00:44:59

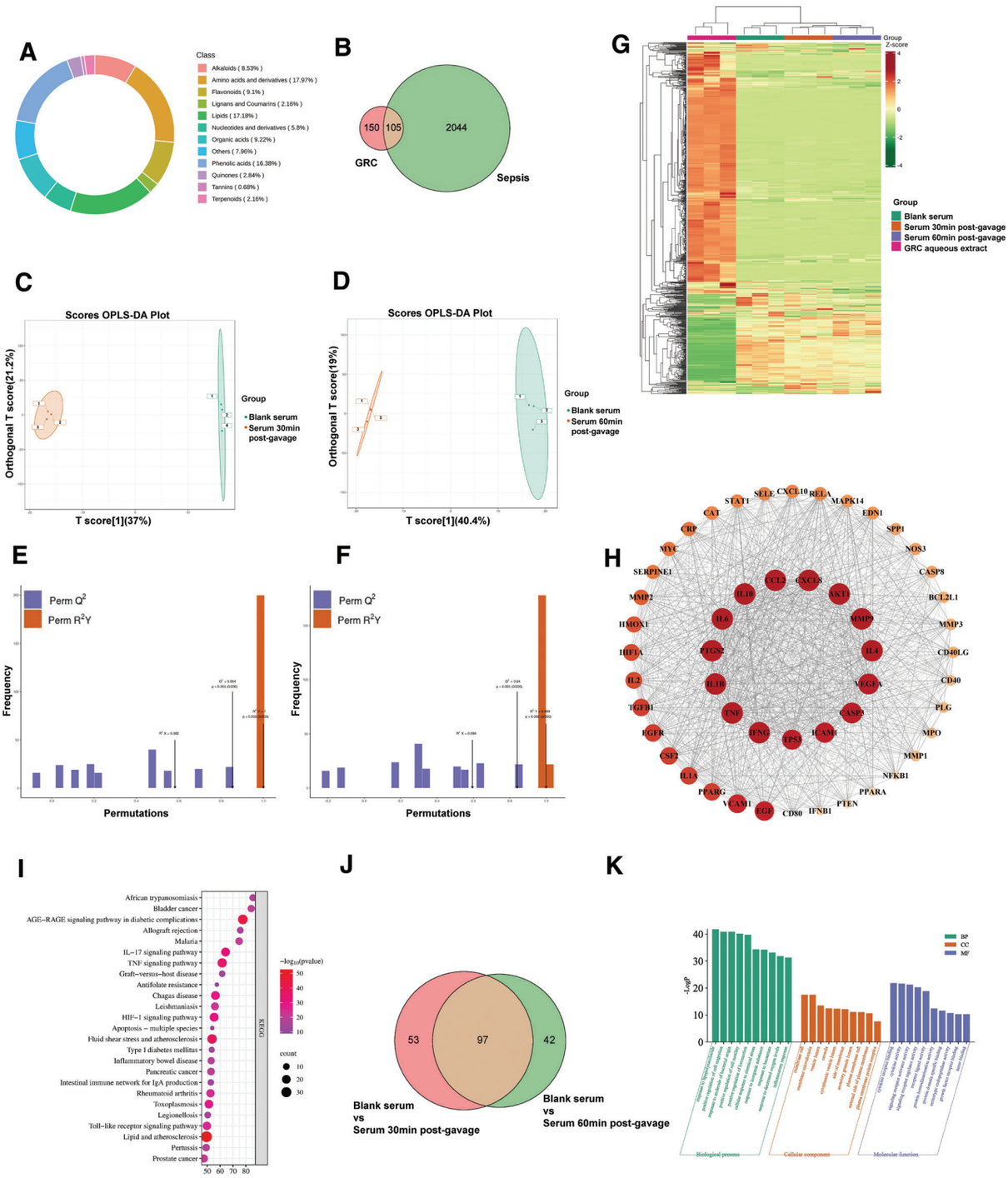


Figure 3. UPLC-MS/MS–based metabolomics and network pharmacology reveal the potential targets and pathways involved in the anti-sepsis mechanism of GRC. (A) Classification of the 879 metabolites detected by UPLC-MS/MS. (B) Venn diagram illustrating the intersection between targets of medicated serum components and sepsis-related targets. (C, D) OPLS-DA score plots showing separation of metabolic profiles among groups. (E, F) Validation plots confirming model robustness without overfitting. (G) Heatmap displaying clustering patterns of metabolites across experimental groups. (H) PPI network of the 105 core targets associated with GRC treatment in sepsis. (I) KEGG pathway enrichment analysis of core targets. (J) Identification of 192 components in medicated serum. (K) GO functional enrichment analysis highlighting terms related to inflammation, hypoxia, bacterial infection, and cytokine activity. GO: Gene Ontology; GRC: Ginseng and Rhubarb Combination; HIF-1: Hypoxia-inducible factor-1; IL: Interleukin; KEGG: Kyoto Encyclopedia of Genes and Genomes; MS: Mass spectrometry; OPLS-DA: Orthogonal partial least squares-discriminant analysis; PPI: Protein–protein interaction; TNF: Tumor necrosis factor; UPLC: Ultra-performance liquid chromatography.

Integrated analysis reveals GRC suppresses ferroptosis by regulating HIF-1 signaling via CaMKII/HO-1

Spearman's correlation analysis revealed significant associations between differential metabolites and proteins in PICS model mice compared to sham controls. Oxoadipic acid was positively correlated with proteins such as IGLC2 and IGLC3 and negatively correlated with RBP4 and GAL. IGLC3 was positively correlated

HM9_V6N2.indb 212 25-Jun-26 00:45:00

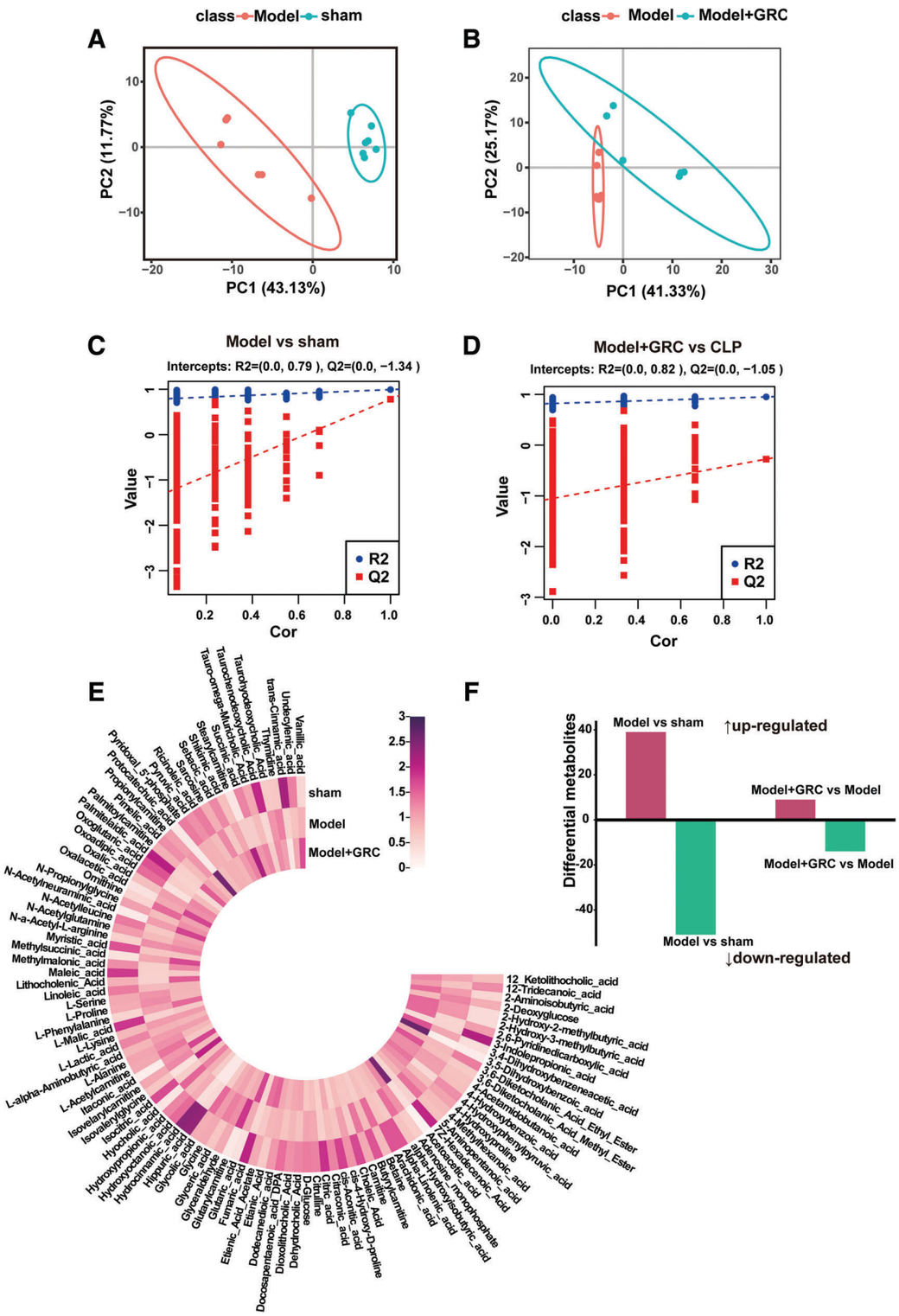


Figure 4. UPLC-MS/MS–based metabolomic profiling reveals GRC-mediated modulation of key metabolic pathways. (A, B) PLS-DA score plots showing distinct metabolic profiles among groups. (C, D) Permutation tests validating model robustness and excluding overfitting. (E) Significantly altered metabolites between groups were identified by univariate analysis. (F) Bar graph showing the count of differential metabolites between groups. GRC: Ginseng and Rhubarb Combination; MS: Mass spectrometry; PLS-DA: Partial least squares-discriminant analysis; UPLC: Ultra-performance liquid chromatography.

with metabolites such as pyruvic acid and succinic acid and negatively correlated with taurohyodeoxycholic acid (Figure 6A and Supplementary Figure S5, https://links.lww.com/AHM/A209). In GRC-treated mice, 2-deoxyglucose was positively correlated with LYPLA1 and transgelin, whereas 4-hydroxyphenylpyruvic acid was positively correlated with FAM3C and IGHV1-59. Oxoadipic acid was negatively correlated with SNRPG, and PAI1 was positively correlated with propionylcarnitine and glycine (Figure 6B).

HM9_V6N2.indb 213 25-Jun-26 00:45:02

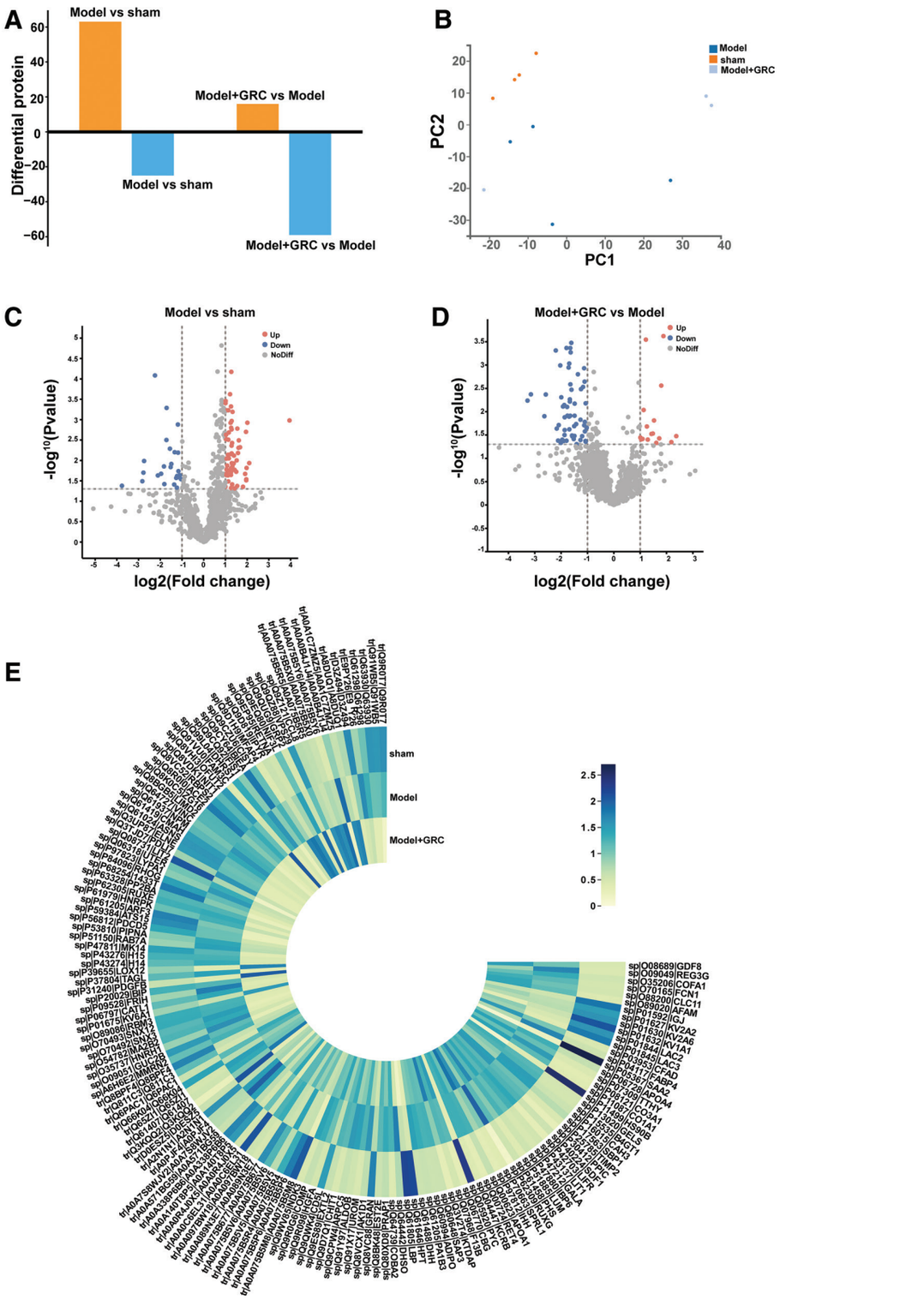


Figure 5. DIA-based quantitative proteomics identifies GRC-mediated reversal of key protein expression patterns in PICS mice. (A) Overview of differentially expressed proteins across experimental groups. (B) PCA showing distinct proteomic profiles among the three groups. (C–E) Differential expression analysis using DIA-based proteomics. DIA: Data-independent acquisition; GRC: Ginseng and Rhubarb Combination; PCA: Principal component analysis; PICS: Persistent inflammatory immunosuppressed catabolic syndrome.

Integrated multi-omics analysis indicated that, although metabolomic data showed clear separation in univariate PCA, proteomic data exhibited only partial separation. However, the combined PCA achieved complete separation between the GRC-treated and PICS model groups, significantly improving classification efficacy (Figure 6C). CCA further confirmed positive correlations between downregulated metabolites (eg, L-proline and carnitine) and downregulated proteins (eg, FABP4 and SNRPG), as well as between upregulated

HM9_V6N2.indb 214 25-Jun-26 00:45:03

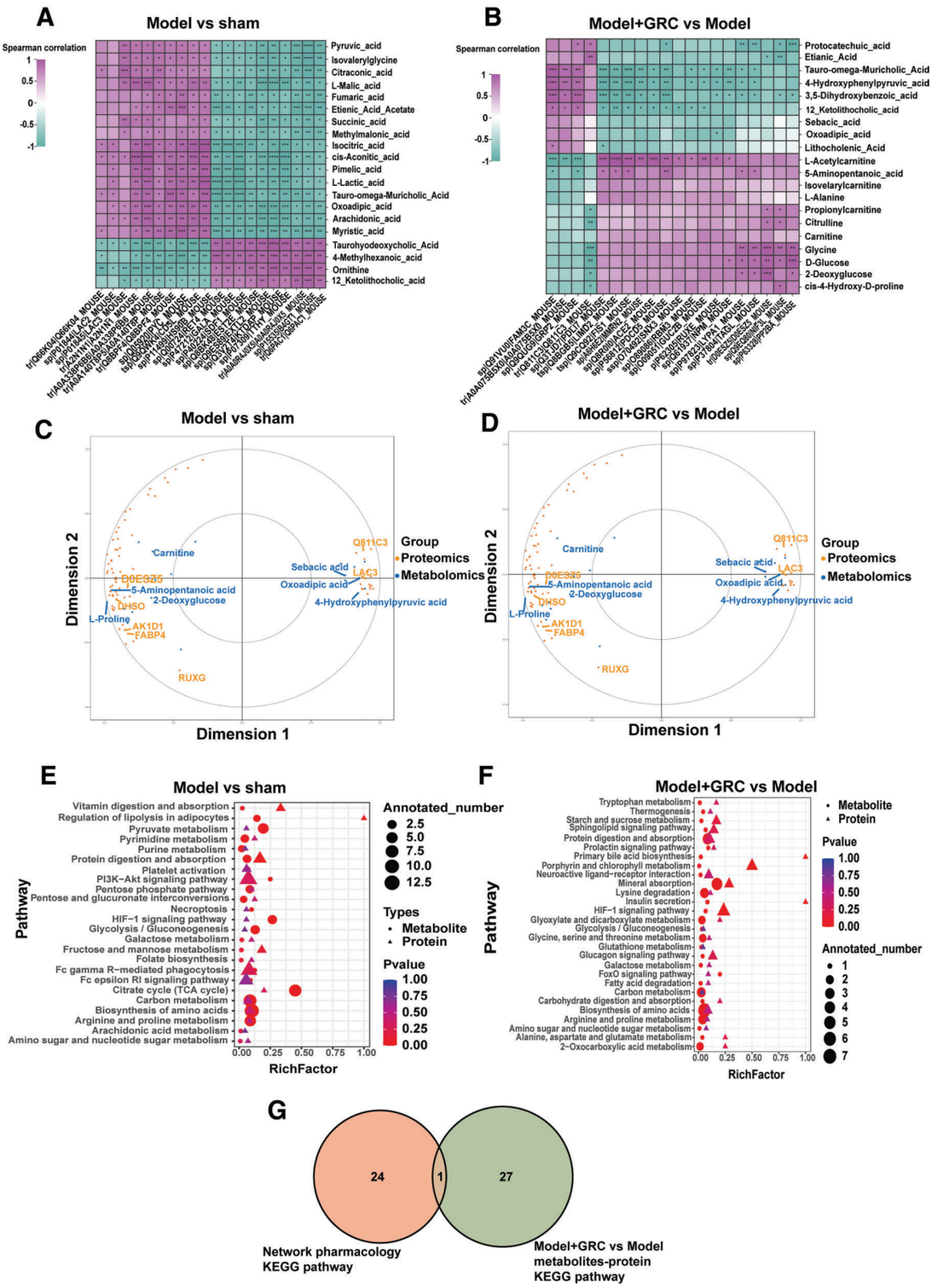


Figure 6. Integrated metabolomic and proteomic analysis reveals GRC suppresses ferroptosis in PICS mice *via* the CaMKII/HO-1 axis of the HIF-1 signaling pathway. (A, B) Spearman correlation analysis of metabolite–protein associations across experimental groups. (C, D) CCA reveals positive correlations between downregulated metabolites and proteins and between upregulated metabolites and proteins. (E, F) KEGG enrichment analysis highlights HIF-1 signaling, mineral absorption, insulin secretion, and primary bile acid biosynthesis as key pathways affected by GRC. (G) A Venn diagram identifies the HIF-1 signaling pathway with key targets labeled. CaMKII: Calmodulin-dependent protein kinases; CCA: Canonical correlation analysis; GRC: Ginseng and Rhubarb Combination; HIF-1: Hypoxia-inducible factor-1; HO-1: Heme oxygenase-1; KEGG: Kyoto Encyclopedia of Genes and Genomes; PICS: Persistent inflammatory immunosuppressed catabolic syndrome.

HM9_V6N2.indb 215 25-Jun-26 00:45:05

metabolites (eg, 4-hydroxyphenylpyruvic acid) and upregulated proteins (eg, IGLC3) (Figure 6D).

KEGG enrichment analysis identified significant associations with HIF-1 signaling, mineral absorption, and insulin secretion pathways (Figure 6E, F). CaMKII and HO-1 emerged as key targets of the HIF-1 pathway. We speculate that GRC inhibits the CaMKII/HO-1 axis, reducing heme degradation-derived Fe^{2+} and thereby alleviating ferroptosis (Figure 6G). Additionally, AKR1D1 in the primary bile acid biosynthesis pathway may contribute to its therapeutic effects. Notably, both network pharmacology and multi-omics analyses consistently identified the HIF-1 signaling pathway as the core mechanism of GRC treatment in PICS, providing compelling evidence for further investigation.

GRC alleviates ferroptosis in PICS mice by inhibiting the CaMKII/HO-1 pathway

The results showed that GRC treatment significantly improved the survival rate of PICS mice. However, this protective effect was markedly attenuated after the addition of OA or CELA ($P = 0.015$, Figure 7A). Histological analysis revealed that GRC treatment effectively mitigated lung structural damage and inflammatory cell infiltration, whereas the introduction of agonists compromised this protective effect (Figure 7M–Q).

Regarding inflammatory cytokines, GRC treatment significantly reduced the expression of pro-inflammatory cytokines (IL-1β, IL-2, IL-5, IL-6, IL-18, TNF-α) and anti-inflammatory cytokines (IL-4, IL-13), whereas the addition of agonists reversed this trend (Figure 7B–I). Assessment of ferroptosis-related indicators demonstrated that GRC intervention significantly decreased Fe^{2+} and MDA levels while enhancing GSH-PX and GPX4 activity. In contrast, agonist treatment completely reversed these changes (Figure 7R–V). Western blot (WB) analysis further confirmed that GRC treatment significantly suppressed the expression of CaMKII and HO-1, whereas agonist administration restored their expression levels (Figure 7J–L).

To further validate this mechanism, we used KN-93, a specific CaMKII inhibitor. The experimental results indicated that CaMKII inhibition effectively restored the balance of oxidative stress and alleviated lipid peroxidation and ferroptosis. WB analysis showed that KN-93 treatment not only reduced the expression of CaMKII and HO-1 but also significantly increased GPX4 protein levels [Supplementary Figure S1A–D, https://links.lww.com/AHM/A209]. These findings confirmed the critical role of CaMKII inhibition in mitigating ferroptosis and protecting organ function. In conclusion, this study demonstrated that GRC effectively alleviated ferroptosis and inflammatory responses by inhibiting the CaMKII/HO-1 signaling pathway, thereby improving the prognosis of PICS mice. Activation of this pathway significantly diminished the protective effects of GRC, suggesting that CaMKII/HO-1 was a key target of GRC in the treatment of PICS.

Discussion

In this study, we established the septic PICS animal model *via* CLP that exhibited pathological features of sustained inflammation, immunosuppression, and catabolism. Integrated metabolomic, proteomic, and network pharmacology analyses revealed that GRC modulates the CaMKII/HO-1 axis within the HIF-1 signaling pathway, thereby inhibiting ferroptosis and reversing the aberrant expression of key PICS-related proteins and metabolic dysregulation. Experimental results demonstrated that GRC treatment not only significantly improved survival rates in PICS mice but also alleviated organ damage and inflammatory responses and effectively reversed immunosuppression. These findings provided compelling experimental evidence supporting GRC as a potential therapeutic strategy for PICS and highlight its novel mechanism of action through multi-target and multi-pathway regulation.

PICS leads to chronic critical conditions in the late stages of sepsis, increasing the risk of secondary infections, prolonging hospital stay, and raising dependence on antibiotics, vasoactive drugs, and mechanical ventilation[23]. Collectively, these factors contributed to clinical deterioration and are associated with higher mortality rates[24–27]. Based on this understanding, we selected 72 hours post-CLP (late-stage sepsis) as the experimental time point, as it exhibited typical PICS characteristics that were significantly different from the pathological features observed in the early stages (6, 12, and 24 hours). Notably, flow cytometric analysis revealed a significant reduction in both $CD4^+$ and $CD8^+$ T cells in the spleens of PICS mice, indicating severe impairment of adaptive immune function. This finding provided cellular evidence of an immunosuppressed state during the PICS phase and offers important insights into its pathogenesis. In contrast, GRC treatment significantly restored the numbers of both $CD4^+$ and $CD8^+$ T cells in the spleen, demonstrating its ability to ameliorate PICS-induced T cell exhaustion, which may represent a key mechanism through which GRC reverses the immunosuppressive state. From the perspective of disease progression, early-stage sepsis is primarily characterized by a dominant pro-inflammatory response accompanied by cytokine storms, whereas immunosuppression plays a secondary role. As the disease progresses, persistent infections exacerbate immunosuppression, resulting in a coexisting state of inflammation and immune dysregulation. Although serum cytokine levels at this stage are lower than the peak observed in early sepsis, the liver continues to produce substantial amounts of both pro-inflammatory and anti-inflammatory factors, accompanied by significant suppression of T cell function. This pattern suggests that, without effective intervention, patients face a poor prognosis.

An in-depth investigation of the mechanisms underlying PICS has important clinical implications for understanding the progression of sepsis. Through integrated multi-omics analyses, our systematic study identified the HIF-1 signaling pathway, CaMKII/HO-1 axis, and ferroptosis as key contributors to PICS pathogenesis. A literature review reveales that ferroptosis, an iron-dependent, non-apoptotic form of cell death, contributes substantially to sepsis-related complications, particularly acute lung injury, cardiac dysfunction, and encephalopathy. Ferroptosis also affects immune responses, metabolic

HM9_V6N2.indb 216 25-Jun-26 00:45:05

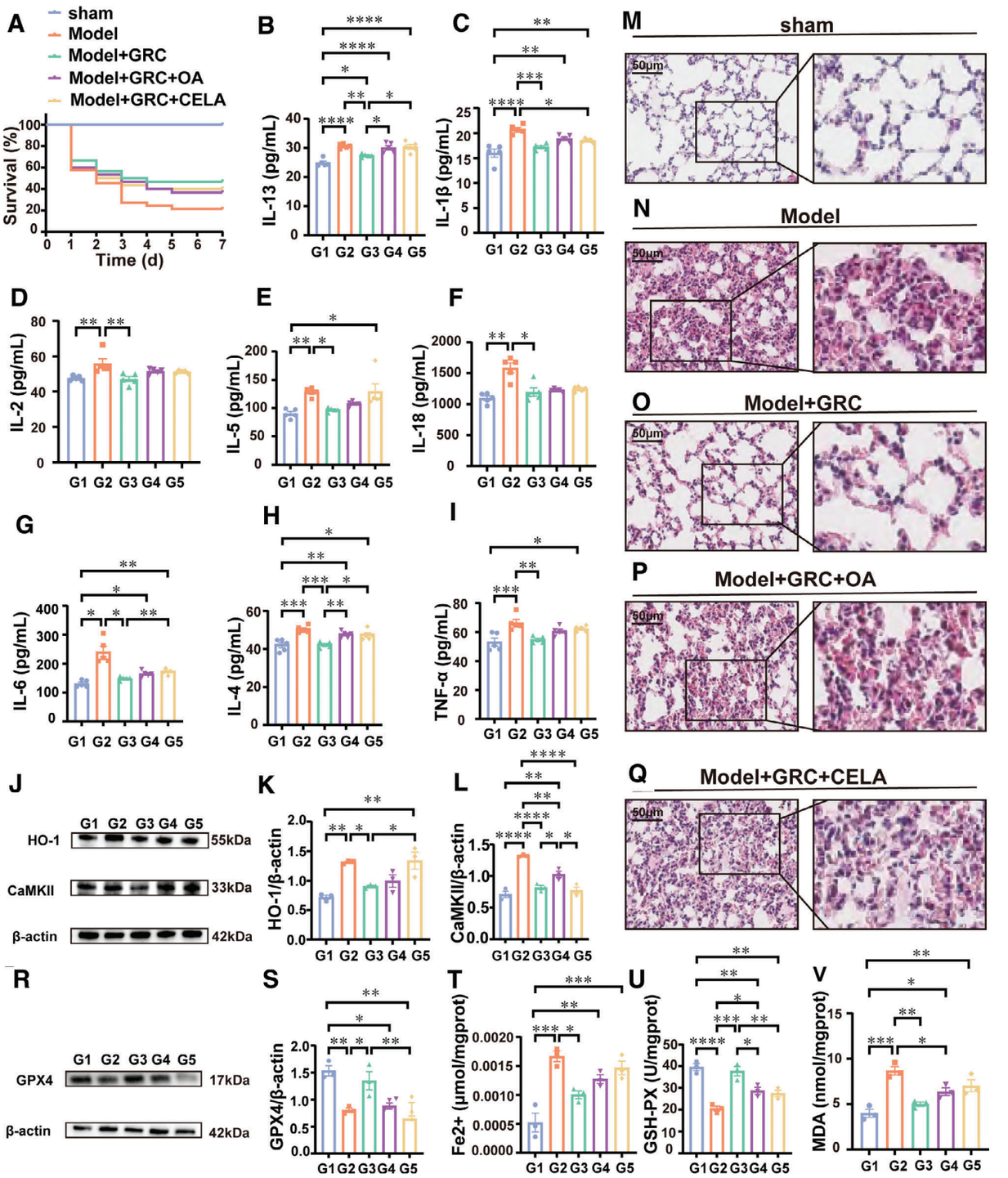


Figure 7. GRC attenuates ferroptosis in PICS mice by inhibiting the CaMKII/HO-1 pathway. (A) Kaplan-Meier survival analysis during 7-day observation. (B–I) Serum levels of IL-1β (B), IL-2 (C), IL-5 (D), IL-6 (E), IL-18 (F), TNF-α (G), IL-4 (H), and IL-13 (I). (J) Representative WB of CaMKII and HO-1 in mouse lung tissue. (K, L) Semiquantitative analysis of HO-1 (K) and CaMKII (L) protein levels. (M–Q) Representative lung histopathology images in the sham group (M), model group (N), model + GRC group (O), model + GRC + OA group (P), and model + GRC + CELA group (Q). (R) Representative WB of GPX4 in mouse lung tissue. (S) Semiquantitative analysis of GPX4 protein levels. (T–V) Fe^{2+} (T), GSH-PX (U), and MDA (V) expression in lung tissues (G1, sham; G2, model; G3, model + GRC; G4, model + GRC + OA; G5, model + GRC + CELA). *$P < 0.05$, **$P < 0.01$, ***$P < 0.001$, ****$P < 0.0001$. CaMKII: Calcium/calmodulin-dependent protein kinase II; CELA: Celastrol; GRC: Ginseng and Rhubarb Combination; GSH-PX: Glutathione peroxidase; HO-1: Heme oxygenase-1; IL: Interleukin; MDA: Malondialdehyde; OA: Oleic acid; PICS: Persistent inflammatory immunosuppressed catabolic syndrome; TNF-α: Tumor necrosis factor-alpha; WB: Western blot.

homeostasis, and oxidative stress levels[28], highlighting its relevance to PICS pathology. CaMKII, a multifunctional serine/threonine protein kinase, not only regulates programmed necrosis but also modulates ferroptosis[29]. Meanwhile, HO-1 promotes ferroptosis by degrading heme to generate free Fe^{2+} and facilitating fatty acid

HM9_V6N2.indb 217 25-Jun-26 00:45:06

peroxidation[30–31]. Our findings demonstrate that GRC treatment effectively downregulates CaMKII/HO-1 expression, reduces Fe^{2+} accumulation, and enhances antioxidant defense mechanisms (evidenced by elevated GSH-PX and GPX4). Conversely, activation of this pathway with OA or CELA abolished these protective effects, whereas the inhibition of CaMKII with KN-93 increased GPX4 expression and alleviated ferroptosis. These results collectively confirm that GRC exerts its therapeutic effects by suppressing ferroptosis through the CaMKII/HO-1 pathway.

Nevertheless, this study has several limitations. First, the role of the CaMKII/HO-1 pathway in sepsis remains relatively unexplored. However, the strength of multi-omics analyses lies precisely in its capacity to uncover previously underappreciated pathways, and our experimental validation confirmed its functional significance. Second, although we utilized *in vivo* inhibitors and agonists for mechanistic exploration, future studies could benefit from employing genetically modified animal models to provide more direct evidence. Finally, the molecular changes identified through metabolomic and proteomic analyses rely primarily on literature-based interpretations, necessitating further functional validation in subsequent experiments.

Conclusions

This study systematically elucidated the multi-target mechanisms of GRC in the treatment of sepsis-associated PICS using integrated metabolomics, proteomics, and network pharmacology. These results demonstrate that GRC effectively inhibits ferroptosis by regulating the CaMKII/HO-1 axis within the HIF-1 signaling pathway, while simultaneously correcting the aberrant expression of key proteins and metabolic disturbances in PICS. Our study not only clarifies the molecular mechanisms through which GRC exerts therapeutic effects *via* multiple targets and pathways but also provides new theoretical and experimental support for developing effective strategies against sepsis-induced PICS, although the role of the CaMKII/HO-1 pathway in sepsis requires further exploration.

Conflict of interest statement

The authors declare no conflict of interest.

Funding

This work was supported by grants from the National Natural Science Foundation of China (82474428, 82505482), National Major Science and Technology Project (2025ZD01903000), and Sanming Project of Medicine in Shenzhen (No. SZZYSM202411012).

Author contributions

Xiaolong Xu and Qingquan Liu designed the study, interpreted data, and supervised the study. Yiming Wei performed experiments, analyzed data, drafted, and edited the manuscript. Xiaomeng Guo drafted and edited the manuscript. Yahui Hu and Yake Li assisted in performing animal experiments. Tengfei Chen assisted in data analysis. Chang Liu, Lixuan Zhang, and Qing Ye assisted in data visualization. All authors reviewed and approved the manuscript.

Ethical approval of studies and informed consent

All animal experiments were performed in accordance with the Guidelines for the Care and Use of Laboratory Animals and were approved by Beijing Hospital of Traditional Chinese Medicine Affiliated to Capital Medical University (BJTCM-M-2024-02-10).

Acknowledgments

The authors thank the Beijing Institute of Traditional Chinese Medicine for the great support with this study.

Data availability

All data from this study is available from the corresponding authors upon reasonable request.

Declaration of Generative AI in Scientific Writing

No generative artificial intelligence (AI) tools were used in the preparation of this manuscript.

References

[1] Rudd KE, Johnson SC, Agesa KM, et al. Global, regional, and national sepsis incidence and mortality, 1990–2017: analysis for the global burden of disease study. *Lancet* 2020;395(10219):200–211.
[2] Xie J, Wang H, Kang Y, et al. The epidemiology of sepsis in Chinese ICUs: a national cross-sectional survey. *Crit Care Med* 2020;48(3):e209–e218.
[3] Chen DK, Hu JM, Yang SJ, et al. Mechanistic studies of the beneficial effects of Anshen Dingzhi prescription for PTSD treatment: roles of the FKBP5-IKKα-NF-κB-NLRP3 signaling pathway. *Acupunct Herb Med* 2025;5(3):316–327.
[4] Xu X, Yan Y, Zheng M, et al. Emodin alleviates sepsis-induced multiorgan damage by inhibiting NETosis through targeting neutrophils BCL-10. *Adv Sci (Weinh)* 2025;12(41):e17129.
[5] Wu JZ, Ma Z, Zhang YH, et al. Precise subcellular organelle-targeted analyses of the hepatotoxicity of rhubarb. *Acupunct Herb Med* 2024;4(2):243–256.
[6] Li SL, Zhang S, Fu L, et al. Chemical Structure and Beneficial Roles of Active Biomacromolecules from Ginseng: A Narrative Review. *Acupunct Herb Med* 2025;5(3):366–378.
[7] Osuchowski MF, Welch K, Siddiqui J, et al. Circulating cytokine/inhibitor profiles reshape the understanding of the SIRS/CARS continuum in sepsis and predict mortality. *J Immunol* 2006;177(3):1967–1974.
[8] Osuchowski MF, Craciun F, Weixelbaumer KM, et al. Sepsis chronically in Mars: systemic cytokine responses are always mixed regardless of the outcome, magnitude, or phase of sepsis. *J Immunol* 2012;189(9):4648–4656.
[9] Gentile LF, Cuenca AG, Efron PA, et al. Persistent inflammation and immunosuppression: a common syndrome and new horizon for surgical intensive care. *J Trauma Acute Care Surg* 2012;72(6):1491–1501.
[10] Chadda KR, Puthucheary Z. Persistent inflammation, immunosuppression, and catabolism syndrome (PICS): a review of definitions, potential therapies, and research priorities. *Br J Anaesth* 2024;132(3):507–518.
[11] Liu R, Li F, Hao S, et al. Low-dose olaparib improves septic cardiac function by reducing ferroptosis *via* accelerated mitophagy flux. *Pharmacol Res* 2024;200:107056.
[12] Wu D, Spencer CB, Ortoga L, et al. Histone lactylation-regulated METTL3 promotes ferroptosis *via* m6A-modification on ACSL4 in sepsis-associated lung injury. *Redox Biol* 2024;74:103194.
[13] Kai L, Song C, Gao M, et al. Uridine alleviates sepsis-induced acute lung injury by inhibiting ferroptosis of macrophage. *Int J Mol Sci* 2023;24(6):5093.

HM9_V6N2.indb 218 25-Jun-26 00:45:06

[14] Tang D, Chen X, Kang R, et al. Ferroptosis: molecular mechanisms and health implications. *Cell Res* 2021;31(2):107–125.
[15] Zhang B, Xiao Q, Ma Q, et al. Clinical treatment for persistent inflammation, immunosuppression and catabolism syndrome in patients with severe acute pancreatitis (review). *Exp Ther Med* 2023;26(4):495.
[16] Zhao Q, Bucchi A, Duan X, et al. Traditional chinese medicine for long COVID-19: the potential roles of immunity remodeling. *Acupunct Herb Med* 2025;5(4):400–419.
[17] Chen Y, Zhang R, Song Y, et al. RRLC-MS/MS-based metabonomics combined with in-depth analysis of metabolic correlation network: finding potential biomarkers for breast cancer. *Analyst* 2009;134(10):2003–2011.
[18] Fraga CG, Clowers BH, Moore RJ, et al. Signature-discovery approach for sample matching of a nerve-agent precursor using liquid chromatography-mass spectrometry, XCMS, and chemometrics. *Anal Chem* 2010;82(10):4165–4173.
[19] Xiao JF, Zhou B, Ressom HW. Metabolite identification and quantitation in LC-MS/MS-based metabolomics. *Trends Anal Chem* 2012;32:1–14.
[20] Szymańska E, Saccenti E, Smilde AK, et al. Double-check: validation of diagnostic statistics for PLS-DA models in metabolomics studies. *Metabolomics* 2012;8(Suppl 1):3–16.
[21] Thévenot EA, Roux A, Xu Y, et al. Analysis of the human adult urinary metabolome variations with age, body mass index, and gender by implementing a comprehensive workflow for univariate and OPLS statistical analyses. *J Proteome Res* 2015;14(8):3322–3335.
[22] Pugh AM, Auteri NJ, Goetzman HS, et al. A murine model of persistent inflammation, immune suppression, and catabolism syndrome. *Int J Mol Sci* 2017;18(8):1741.
[23] Mira JC, Gentile LF, Mathias BJ, et al. Sepsis pathophysiology, chronic critical illness, and persistent inflammation-immunosuppression and catabolism syndrome. *Crit Care Med* 2017;45(2):253–262.
[24] Suganuma S, Idei M, Nakano H, et al. Impact of persistent inflammation, immunosuppression, and catabolism syndrome during intensive care admission on each post-intensive care syndrome component in a PICS clinic. *J Clin Med* 2023;12(16):5427.
[25] Mankowski RT, Anton SD, Ghita GL, et al. Older adults demonstrate biomarker evidence of the persistent inflammation, immunosuppression, and catabolism syndrome (PICS) after sepsis. *J Gerontol A Biol Sci Med Sci* 2022;77(1):188–196.
[26] Hesselink L, Hoepelman RJ, Spijkerman R, et al. Persistent inflammation, immunosuppression and catabolism syndrome (PICS) after polytrauma: a rare syndrome with major consequences. *J Clin Med* 2020;9(1):191.
[27] Hauschild DB, Oliveira LDA, Ventura JC, et al. Persistent inflammation, immunosuppression and catabolism syndrome (PICS) in critically ill children is associated with clinical outcomes: a prospective longitudinal study. *J Human Nutr Dietetics* 2021;34(2):365–373.
[28] Li XL, Zhang GY, Guo R, et al. Ferroptosis in sepsis: the mechanism, the role and the therapeutic potential. *Front Immunol* 2022;13:956361.
[29] Zhang M, Gao H, Liu D, et al. CaMKII-δ9 promotes cardiomyopathy through disrupting UBE2T-dependent DNA repair. *Nat Cell Biol* 2019;21(9):1152–1163.
[30] Han S, Lin F, Qi Y, et al. HO-1 contributes to luteolin-triggered ferroptosis in clear cell renal cell carcinoma *via* increasing the labile iron pool and promoting lipid peroxidation. *Oxid Med Cell Longevity* 2022;2022:3846217.
[31] Zhang X, Xu X, Liu H, et al. CCR2-overexpressing biomimetic carrier-free nanoplatform for enhanced cascade ferroptosis tumor therapy. *Acta Biomater* 2023;166:604–614.

HM9_V6N2.indb 219 25-Jun-26 00:45:06